HHS Public Access

Author manuscript

Nat Genet. Author manuscript; available in PMC 2010 March 01.

Published in final edited form as:

Nat Genet. 2009 September ; 41(9): 977–985. doi:10.1038/ng.435.

Posterior Malformations in *Dact1* mutant mice arise through misregulated Vangl2 at the Primitive Streak

Rowena Suriben[1,2,*], **Saul Kivimäe**[1,*], **Daniel A. Fisher**[1,*], **Randall T. Moon**[4], and **Benjamin N.R. Cheyette**[1,2,3]

[1]Department of Psychiatry, University of California San Francisco, 1550 4th St, San Francisco, CA, 94158, USA

[2]Graduate Program in Developmental Biology, University of California San Francisco, 1550 4th St, San Francisco, CA, 94158, USA

[3]Graduate Program in Neuroscience, University of California San Francisco, 1550 4th St, San Francisco, CA, 94158, USA

[4]Howard Hughes Medical Institute, Institute for Stem Cell and Regenerative Medicine, and Department of Pharmacology, University of Washington School of Medicine, Seattle WA, 95195, USA

Abstract

Mice homozygous for mutations in *Dact1 (Dpr/Frodo)* phenocopy human malformations involving the spine, genitourinary system, and distal digestive tract. We trace this phenotype to disrupted germ layer morphogenesis at the primitive streak (PS). Remarkably, heterozygous mutation of *Vangl2*, a transmembrane component of the Planar Cell Polarity (PCP) pathway, rescues recessive *Dact1* phenotypes, whereas loss of *Dact1* reciprocally rescues semidominant *Vangl2* phenotypes. We show that Dact1, an intracellular protein, forms a complex with Vangl2. In *Dact1* mutants, Vangl2 is increased at the PS where cells ordinarily undergo an epithelial-mesenchymal transition. This is associated with abnormal E-cadherin distribution and changes in biochemical measures of the PCP pathway. We conclude that Dact1 contributes to morphogenesis at the PS by regulating Vangl2 upstream of cell adhesion and the PCP pathway.

Keywords

Dact (Dapper Frodo); Vangl2 (Van Gogh Strabismus); PCP; Wnt; spina bifida; caudal regression; OEIS; primitive streak

Correspondence should be addressed to B.N.R.C. (benjamin.cheyette@ucsf.edu).

*These authors contributed equally to this work.

AUTHOR CONTRIBUTIONS R.S. contributed gene expression, QPCR (Wnt signaling targets), most embryological analyses, confocal microscopy, and genetics. S.K. contributed antigen synthesis, antibody characterization, Western blots, kinase assays, coIPs, pull-downs, and associated plasmid constructs. D.A.F. contributed skeletal and somitogenic analyses, BAT-gal WISH, and genetics including the initial $Vangl2^{Lp}$ cross. B.N.R.C. designed the *Dact1* targeting construct in the laboratory of R.T.M. at the UW. The experiments of R.S., S.K., and D.A.F. were performed at UCSF in the laboratory of B.N.R.C., who supervised this research and wrote the text with feedback from all authors.

Multiple developmental events occur at or within close proximity to the primitive streak (PS) in the posterior embryo. These include epithelial-mesenchymal transition (EMT) associated with specification of primary germ layers, ventral closure of endoderm to form hindgut, medial-lateral division of mesoderm, posterior elongation of the notochord, segment formation, and dorsal closure of neuroectoderm to form the neural tube. Planar Cell Polarity (PCP) and Wnt/β-catenin signaling are both involved in these processes1-4.

Vangl2 (Van Gogh-like/Strabismus) is a four-pass-transmembrane protein that plays a major role in the PCP pathway. By establishing asymmetric localization of both membrane and cytoplasmic components, this pathway regulates cell polarity and movements, particularly convergent-extension (CE) movements that shape germ layer derivatives shortly after gastrulation at the PS5. Vangl proteins directly interact with the intracellular protein Dishevelled (Dvl), a central component of both the PCP and Wnt/ß-catenin signaling pathways6. The Wnt/β-catenin pathway is mechanistically distinct from PCP; it determines cell decisions by regulating transcriptional activity of target genes downstream of post-translational stabilization of the β-catenin protein7.

Mice with mutations affecting each of these pathways have phenotypes linked to events in the PS region. For example, mutations in *Wnt3a*, a posterior patterning ligand that activates the Wnt/β-catenin pathway, cause posterior truncation stemming from defective mesoderm specification1. Mutations in *Vangl* family members that diminish PCP activity cause neural tube defects traced to defective cell movements in the neuroectoderm2. Despite established roles in both these pathways in other systems, *Dvl* mutations have so far been linked only to PCP phenotypes in mice8.

Dact (Dapper/Frodo) proteins bind Dvl and have been shown to modulate several signaling pathways, including Wnt/β-catenin signaling9-13. By studying an engineered mutation in mouse *Dact1*, we have discovered strong and reciprocal genetic interactions with *Vangl2*. Biochemical and embryonic analyses reveal that this unusual genetic relationship reflects a role for Dact1 in post-translational regulation of Vangl2 at the PS, upstream of cell adhesion and PCP signaling.

RESULTS

A spectrum of posterior birth defects in *Dact1* mutant mice

We genetically engineered an allelic series at the mouse *Dact1* locus including two equally severe alleles deduced to be *nulls* on molecular and biochemical grounds (Supplementary Fig 1). One allele ($Dact1^{neo\Delta}$) was backcrossed for more than ten generations to the C57BL/6 isogenic mouse strain for use in this study; these homozygotes are hereafter referred to as *Dact1* mutants.

Dact1 mutants are born at near Mendelian ratios (Supplementary Table 1a), but with rare exceptions die within a day of birth. These neonates have a short tail, no anus, no urinary outlet, nor external genitalia (Fig 1a-d). Internally, the vast majority have blind-ended colons (Fig 1e-f) and no bladder (Fig 1g-h, Supplementary Table 1b). Ureters are present but connect at the midline or fuse with the reproductive ducts, while the kidneys are invariably

hydronephrotic (Fig 1h). The kidneys also display variable developmental malformations ranging from fusion at the midline to complete agenesis (Fig 1h, Supplementary Table 1c). Rare mutants (<1%) that survive postnatally nonetheless have non-lethal genitourinary and digestive tract abnormalities evident upon laparotomy (Fig 1i-k). Gonads of mutants of both sexes are typically present and grossly normal (Fig 1h).

In addition to genitourinary and gastrointestinal phenotypes, most (~90%) *Dact1* mutants are immediately distinguishable from littermates by virtue of segmental truncation (Fig 1a-b; Supplementary Table 1d). Skeletal analysis reveals segmental loss that is most commonly (73%) restricted to the tail (Fig 1l-m; o-p). A smaller percentage (17%) has truncations extending into sacral and lumbar regions (Fig 1n, q); these are rarely accompanied by malformations of the pelvis and hindlimbs, including sirenomelia (Fig 1r). Most severely truncated mutants have spina bifida (13% of total; Fig 1s). Although there are usually a few smaller malformed vertebrae immediately anterior to the segmental truncation, all other vertebrae and ribs are of normal size, morphology, and identity (Fig 1p-q). Since segmentation in vertebrates proceeds from anterior to posterior15, the striking lack of anterior segment abnormalities in *Dact1* mutants suggests segmentation failure restricted to late developmental stages, as opposed to a more general disruption of this process16,17.

Embryonic defects in *Dact1* mutants

The earliest developmental differences we detect in *Dact1* mutants occur at embryonic day (E) 8.25, shortly after segmentation begins when the embryo has 4-7 newly formed somites15. Unstained wild type and mutant embryos are indistinguishable anteriorly (Fig 2a-b), and whole mount mRNA in situ hybridization (WISH) using an Uncx4.1 probe that marks the posterior compartment of each segment16, demonstrates that somites are normal (Fig 2a-b insets) at this stage. Nonetheless, *Dact1* mutants are misshapen posteriorly in the region of the PS. Viewed dorsally, the wild type embryo has a rounded posterior contour (Fig 2a) whereas *Dact1* mutants are slightly spade shaped: widening abnormally before tapering to a more pointed tip (Fig 2b asterisk). As morphological differences in *Dact1* mutants are confined to the posterior, we quantified them by measuring Length-Width Ratio (LWR) specifically in this region ("Posterior LWR"; **Methods**). Posterior LWR at the 6-7 somite stage is significantly reduced in *Dact1* mutant embryos compared to wild type (1.57 ± 0.05 *vs*. 1.85 ± 0.04, p = 0.0008) (Fig 2c). We also detected a significant reduction compared to wild type in the Posterior LWR of $Vangl2^{Lp/+}$ embryos (1.67 ± 0.04 *vs*. 1.85 ± 0.04, p = 0.0096) (Fig 2c), which are heterozygous for a semidominant allele in *Vangl2*18. Consistent with a prior report3, using LWR based on the whole embryo ("whole embryo LWR"; **Methods**), we detected no significant differences between wild type (9.42 ± 0.23) and $Vangl2^{Lp/+}$ (9.05 ± 0.36; p = 0.4) at the 6-7 somite stage, nor between wild type and *Dact1* mutants (9.48 ± 0.43; p = 0.9) (Fig 2d). Since CE movements in the posterior embryo have been shown to be affected in $Vangl2^{Lp/+}$ embryos at this stage4, our findings suggest that Posterior LWR reflects cell movements within this embryonic region, and that these are disrupted in *Dact1* mutants.

We next used a panel of WISH markers to assess morphology of individual tissues in this region. Viewed from either the ventral or lateral aspect, WISH for Shh shows that the

presumptive notochord domain19 is broader in *Dact1* mutants and does not extend as far posteriorly beyond the last-formed somite (labeled by Uncx4.1 WISH) (Fig 2e-h). There are also differences in morphology of the posterior endoderm, which like the presumptive notochord domain does not extend as far posteriorly and is delayed in folding ventrally to form the hindgut diverticulum (Fig 2g-h). Presomitic mesoderm labeled with Dll1 is normal in volume but is redistributed around the shortened axial and ventral structures (Fig 2i-j). Unlike the shortened axial mesoderm and endoderm, the ectoderm in *Dact1* mutants extends to the posterior tip of the embryo, even in mutants where ventral defects are severe (Fig 2i-j arrows).

Consistent with these WISH data, cross section at the PS reveals that all three germ layers are present in the posterior *Dact1* mutant embryo at the 6 somite stage, but there is a notable divergence from wild type morphology. The endoderm is open ventrally and fails to form a tubular hindgut with columnar epithelium (Fig 2k-l). Ectoderm morphology is variable but is often 1 to 2 cells thicker apical-basally, and is more acutely folded (Fig 2k-l insets & asterisk). Rates of proliferation and cell death are not significantly different in this region even in mutants with severely affected morphology (Supplementary Fig 2).

To investigate how these early morphological defects progress, we examined the development of germ layer derivatives at later stages. At E9.5, presomitic mesoderm expressing Dll1 continues to extend fully posteriorly in mutants, as does the overlying ectoderm (Fig 2m-n). However, axial structures that normally separate left from right presomitic (paraxial) mesoderm terminate more anteriorly, such that this tissue assumes an abnormal Y-instead of a U-shape when viewed dorsally (Fig 2o-p).

The posterior segments that are frequently missing in *Dact1* mutants are generated only after E9.5 from the presomitic mesoderm (PSM) located in the tail bud15. Concordantly, Uncx4.1 WISH reveals segmental defects only after E9.5 and only in the most recently formed somites (Fig 2q-r). Segmentation is governed in part by the somitogenesis cycle, a regular oscillation of gene expression in the PSM, and some mutations that cause segmental loss disrupt this cycle throughout development20. We tested whether *Dact1* mutants have disruptions in the somitogenesis cycle at late stages by examining expression of well-established somitogenesis genes such as *Lfng*16,20. Expression of *Lfng* and other somitogenesis cycle markers was disrupted in *Dact1* mutants by E10.5 (Fig 2s-t; Supplementary Table 2). However, these somitogenesis cycle defects never occurred before E10 and never in isolation: mutant tail buds by this stage invariably displayed extensive anatomical disorganization and evidence of histolysis including absence of the tail gut (posterior endoderm), severe shortening of the notochord, and pockets of pooled blood and serous fluid (Fig 2u-x; Supplementary Table 2).

Taken together, these embryological data suggest that the *Dact1* mutant phenotype arises from a primary defect in germ layer morphogenesis at the PS; segmental truncations in these mutants are associated with failed somitogenesis occurring in the context of tail bud disorganization and deterioration at later stages.

PCP but not Wnt/β-catenin signaling is affected in *Dact1* mutant embryos

Work in other systems has suggested that Dact1 primarily modulates Wnt/β-catenin signaling9,10,12,13. We accordingly asked whether Wnt/β-catenin pathway defects underlie the earliest observable *Dact1* mutant phenotypes in the posterior embryo. We measured Wnt/β-catenin target mRNA levels by Quantitative Reverse Transcriptase PCR (QPCR) at the stage when morphological differences are first detected in *Dact1* mutants (5-7 somites). We validated this assay using previously studied signaling mutants4,17 and the established Wnt/β-catenin targets, Dll1 and Axin221. Levels of both these targets were significantly reduced in posterior tissues from *Wnt3a null* embryos compared to control littermates (% of average wild type for Dll1: 16 ± 2 *vs*. 100 ± 10; $p<0.0001$, for Axin2: 42 ± 7 *vs*. 100 ± 14; p=0.004) (Fig 3a-b). Moreover, levels of these targets were not significantly different in posterior tissues from heterozygotes for the semidominant PCP signaling mutant *Vangl2*^{Lp} (% of average wild type for Dll1: 121 ± 11 *vs*. 100 ± 9; p=0.2, for Axin2: 77 ± 11 *vs*. 100 ± 20; p = 0.3) (Fig 3c-d). *Dact1* mutant posterior tissues showed no significant differences in these Wnt/β-catenin target gene levels compared to controls (% of average wild type for Dll1: 95 ± 8 *vs*. 100 ± 7; p = 0.6, for Axin2: 85 ± 17 *vs*. 100 ± 15; p = 0.5) (Fig 3e-f). Similarly, we measured levels of activated β-catenin protein at E9 by immunoblot with dephospho-specific β-catenin antibody (mAb 8E7)22; there were no significant differences compared to controls (% of average wild type = 81 ± 8 *vs*. 100 ± 10; p = 0.2) (Fig 3g-h). Finally, when assessed by WISH, expression of the posterior Wnt/β-catenin signaling targets *Dll1* and *Brachyury* (*T*) were not significantly reduced in *Dact1* mutant embryos (Fig 2i-j, m-p; Supplementary Fig 3a-b). We also detected no differences in levels of the p120-catenin (Ctnnd1) or Dvl proteins (Supplementary Fig 3c-d), previously shown to be regulated by Dact family members in other contexts9,13,23.

Some of the phenotypes observed in *Dact1* mutants, such as neural tube defects, broadening of the presumptive notochord domain, and differences in posterior LWR, resemble those known to result from PCP pathway disruptions4,24. Among several putative intracellular effectors, PCP signaling is linked to regulation of two kinases: Rho associated kinase4 and c-Jun N-terminal Kinase (JNK)5. We tested whether activities of these kinases are altered in the *Dact1* mutant posterior embryo. To assess Rho kinase activity we used immunoblotting with a phospho-specific antibody to measure amounts of its phosphorylated substrate, Mypt125. In E8 posterior embryo lysates from *Dact1* mutants, levels of phosphorylated Mypt1 were significantly reduced compared to controls (% of average wild type = 69 ± 9 *vs*. 100 ± 8; p = 0.03) (Fig 3i-j). We measured activated JNK in posterior embryo lysates at E9 through direct phosphorylation of a GST-Jun fusion protein normalized against total JNK recovered in a pull-down assay26. Endogenous JNK activity was unambiguously increased in *Dact1* mutant posterior embryos at this stage (% of average wild type = 258 ± 19 *vs*. 99 ± 13; p = 0.0005) (Fig 3k-l).

In summary, molecular, biochemical, and embryonic assays at early phenotypic stages do not support changes in Wnt/β-catenin signaling in *Dact1* mutants; they instead indicate defects in the PCP pathway.

Mutations in *Dact1* and *Vangl2* exhibit reciprocal genetic rescue

In mice, synergy with one copy of *Vangl2*^{Lp} to cause neural tube defects is generally accepted as evidence that a genetic locus participates in the PCP pathway3. Because *Dact1* mutants display a partially penetrant neural tube defect (spina bifida) and also have abnormalities in embryological and biochemical measures associated with PCP signaling, we predicted that mice homozygous for the *Dact1* mutation and heterozygous for *Vangl2*^{Lp} would display severe defects in neural tube closure.

Unexpectedly, mutations in *Dact1* and *Vangl2* mutually rescue each other, such that nearly all *Dact1* mutant mice heterozygous for *Vangl2*^{Lp} appear grossly normal and display neither *Vangl2*^{Lp} semidominant nor *Dact1* recessive phenotypes (Fig 4a-d). From a cross conducted in a 97% isogenic C57Bl/6 genetic background, approximately 80% (9/11) of *Dact1*$^{-/-}$;*Vangl2*$^{Lp/+}$ mice had normal genitourinary (GU) systems, normal gastrointestinal (GI) systems, no segmental truncation, and no neural tube defects, compared to *Dact1*$^{-/-}$;*Vangl2*$^{+/+}$ littermates of which 100% (11/11) had GU phenotypes, 90% (10/11) had GI phenotypes, >50% (6/11) had segmental truncation, and ~20% (2/11) had spina bifida (Fig 4e red *vs*. blue; Supplementary Table 3a). *Vangl2* mutant-mediated rescue of the *Dact1* mutant phenotype is not due to a molecular peculiarity of the *Vangl2*^{Lp} allele because a very similar pattern of rescue is observed with an independently derived allele27, *Vangl2*$^{Lp\text{-}m1Jus}$ (Fig 4e green *vs*. yellow; Supplementary Table 3a). Conversely, whereas more than 80% of animals heterozygous for either *Vangl2*^{Lp} or *Vangl2*$^{Lp\text{-}m1Jus}$ (5/6 & 8/10 respectively) display the characteristic semidominant curly tail (*Looptail*) phenotype, penetrance of this phenotype drops to <65% (11/17 & 9/22 respectively) when animals are heterozygous, and to ≤20% (1/10 & 3/15 respectively) when homozygous, for the *Dact1* mutant allele (Fig 4f; Supplementary Table 3b). Nevertheless, although Dact1 loss rescues the semidominant *Loop-tail* phenotype, it does not rescue the recessive craniorachischesis phenotype of homozygous *Vangl2* mutant embryos (Supplementary Fig 4).

To summarize, genetic experiments demonstrate that recessive *Dact1* mutant phenotypes are abrogated by mutation of one *Vangl2* allele, and conversely that semidominant *Vangl2* mutant phenotypes are ameliorated by loss of Dact1. Failure to rescue the homozygous *Vangl2* mutant phenotype demonstrates that a functional allele of *Vangl2* is required for this reciprocal genetic interaction.

Dact1 and Vangl2 are binding partners

One mechanism whereby Dact1 could regulate Vangl2 is through physical interaction. We tested this hypothesis through a series of co-immunoprecipitation (coIP) and pull-down assays, results of which are schematically summarized in Figure 5a-c.

When co-expressed in human embryonic kidney (HEK 293) cells, the Vangl2 protein coIPs with Dact1 (Fig 5d). We determined the region of Dact1 responsible for this interaction through a panel of Dact1 deletion constructs. Loss of the C-terminal 88 amino acids (aa) of Dact1 almost completely eliminates association with Vangl2, and the residual interaction is abolished by deletion of an additional 62 aa (Fig 5d). Under identical conditions, the same panel of Dact1 constructs shows a different coIP pattern with Dvl2: Progressive C-terminal

deletions of Dact1 reduce but do not eliminate association with Dvl2 until elimination of aa 311-778 (Fig 5e). The Dact1 PDZb caps a longer stretch of 28 highly conserved aa14, and so we made specific deletions to probe how this region compares to the immediately upstream 60 aa in coIPs with Vangl2 versus Dvl2. Deletion of the Dact1 C-terminal 28 aa has no effect on association with Vangl2 (Fig 5f), but reduces association with Dvl2 at least as much as larger deletions (Fig 5g). Conversely, internal deletion of the adjacent 60 aa has no effect on Dact1 association with Dvl2 (Fig 5g), but reduces association with Vangl2 similar to larger deletions (Fig 5f). Taken together these data strongly suggest that separate domains of Dact1 contribute to complex formation with Vangl2 versus Dvl2.

We similarly used a series of Dvl2 deletion constructs to probe whether different conserved regions of Dvl are responsible for associations with Dact1 versus Vangl2. Consistent with prior reports6,28, we found that the Dvl PDZ domain is the main contributor to the Dvl-Vangl2 interaction (Fig 5h). We also found that a “Dishevelled Specific” (DS) domain (**Methods**) contributes modestly to this interaction (Fig 5h). In contrast, using the same panel of Dvl2 constructs under identical conditions we found that deletion of the PDZ and DS domains reduces but does not eliminate the Dvl-Dact1 interaction (Fig 5i). Taken together, these coIP data strongly suggest that besides PDZ-b/PDZ binding12, a middle region of Dact1 also contributes to interactions with Dvl2 outside the PDZ domain, consistent with some prior reports9,10.

These experiments indicate that different domains contribute to associations between Dact1 and Dvl2 versus either of these proteins with Vangl2. In a final assay we asked whether Vangl2 can bind directly to Dact1 in the absence of Dvl proteins. Since Dvl proteins are specific to metazoans, we bacterially expressed and purified recombinant GST fusion proteins corresponding to the amino-and carboxy-terminal regions of Dact1 and asked whether they bind to full-length Vangl2 protein synthesized in a wheat germ extract. The C-terminal half of Dact1 binds specifically to Vangl2 in this Dvl-free system, supporting the conclusion that the Dact1-Vangl2 interaction is direct (Fig 5j).

Dact1 regulates Vangl2 at the PS

By prior report, *Vangl2* is expressed at low levels in the posterior endoderm and at higher levels in the neuroectoderm, which is contiguous with ectoderm in the PS region29,30. Dact1 is expressed in a potentially overlapping domain in the posterior ectoderm and mesoderm31. This suggests that Dact1 and Vangl2 might functionally interact in these tissues, particularly in the PS ectoderm.

Using WISH we confirmed that the mRNA distributions of Dact1 (Fig 6a-b) and Vangl2 (Fig 6c-d) overlap in PS ectoderm. As expected for a transmembrane protein and consistent with prior reports29, an affinity-purified antibody detects Vangl2 protein primarily on surfaces of epithelial cells in the PS ectoderm and endoderm, as well as more weakly on scattered surface subdomains of adjacent mesenchymal cells (Fig 6e inset; arrowheads). The adhesion protein E-cadherin shows a partially overlapping distribution with Vangl2 in all germ layers, but is concentrated at the apical and basal surfaces and is generally less apparent on the lateral membranes of ectoderm cells (Fig 6f-g inset).

In the PS ectoderm of *Dact1* mutants, Vangl2 cell surface signal is significantly increased (Fig 6h; Supplementary Fig 5b; e). Moreover, cell surface E-cadherin is also significantly increased and colocalizes with the Vangl2 signal, no longer displaying enrichment on the apical-basal *vs*. lateral cell surfaces (Fig 6i-j; Supplementary Fig 5b; f). This is a post-translational effect, as levels of both the Vangl2 and E-cadherin mRNAs are not altered (Supplementary Fig 6a-b). In these mutants, cells with high Vangl2 and E-cadherin form a bulge at the position of the PS where EMT normally occurs (Fig 6j dotted lines).

Prior reports suggest that the *Vangl2*^{Lp} mutation alters the ability of mutant Vangl2 protein to stably accumulate at the membrane, especially asymmetrically or at points of cell contact18,32,33. Consistent with this, we find that in *Vangl2*$^{Lp/+}$ embryos, Vangl2 protein remains detectable in cells where the wild type protein is typically expressed, but the membrane signal is significantly reduced compared to wild type (Fig 6k; Supplementary Fig 5c; e). Interestingly, E-cadherin is also mislocalized in these cells: a diffuse cytoplasmic signal appears that is absent from wild type controls (Fig 6l). Nevertheless, some apical-basal enrichment of E-cadherin remains evident (Fig 6l inset), and levels on the lateral edges of PS ectoderm cells are as low as in wild type (Supplementary Fig 5c; f).

The PS ectoderm in *Dact1*$^{-/-}$;*Vangl2*$^{Lp/+}$ combination mutants has Vangl2 cell surface staining intermediate between the high signal detected in *Dact1* mutants and the low signal detected in *Vangl2*$^{Lp/+}$ embryos, such that levels are not significantly different from wild type controls (Fig 6n inset; Supplementary Fig 5d; e). In contrast to *Dact1* single mutants, *Dact1*$^{-/-}$;*Vangl2*$^{Lp/+}$ combination mutants also have normal surface levels and a more normal apical-basal distribution of E-cadherin in PS ectoderm cells (Supplementary Fig 5f; Fig 6o inset). Finally, the bulge of cells with high Vangl2 and E-cadherin found at the PS in *Dact1* single mutants is absent from combination mutants (Fig 6p dotted lines).

To summarize, loss of Dact1 leads to increased Vangl2 and E-cadherin in the PS ectoderm where cells normally undergo EMT. In *Vangl2*^{Lp} heterozygotes, there is partial loss of membrane Vangl2 signal; this most likely reflects the absence of surface-destabilized mutant protein made from the *Loop-tail* allele32. Compared to *Dact1* mutants, *Dact1*$^{-/-}$;*Vangl2*$^{Lp/+}$ combination mutant embryos have partially restored cell surface Vangl2 levels, E-cadherin distribution, and PS morphology.

DISCUSSION

The phenotypic spectrum in *Dact1* mutant mice is reminiscent of a similar spectrum of posterior malformations in humans34. Etiologies previously proposed to explain all or part of this spectrum include vascular-steal35, persistence of the embryonic cloaca36, and defects in posterior mesoderm formation37. Our findings suggest that this malformation spectrum may first originate in disturbed morphogenetic movements at the PS in the early embryo.

Several morphogenetic processes take place in close spatial and temporal proximity in the posterior embryo, each of which is likely to require dynamic regulation and polarized activities of Vangl2, the PCP pathway, and adhesive proteins. The first of these to occur is

EMT at the PS, where both Dact1 and Vangl2 are expressed but where neither protein has a prior established role. Our data suggest that defective EMT is the primary defect in *Dact1* mutants. Perhaps all other disrupted morphogenesis in these mutants occurs secondarily, for example because of decreased generation of mesoderm and endoderm precursors via EMT. Nonetheless we cannot rule out additional requirements for Dact1 alongside Vangl2 in spatially and temporally adjacent morphogenetic events, including CE movements that elongate and narrow axial mesoderm, mesenchymal-epithelial transition of endoderm precursors, or polarity and cell movements that fold and extend the hindgut.

Wnt/β-catenin signaling and E-cadherin negatively regulate each other at the PS, such that high E-cadherin reduces Wnt/β-catenin signal transduction in cells undergoing EMT38, and Wnt/β-catenin signaling reciprocally negatively regulates E-cadherin transcription39. We have observed no statistically significant alterations in Wnt/β-catenin signaling or in levels of E-cadherin mRNA in early *Dact1* mutant embryos. Instead the E-cadherin protein is abnormally redistributed at early stages, whereas Wnt/β-catenin signaling reductions occur only much later in morphologically disrupted tail buds where they might contribute to somitogenesis failure specific to late-forming posterior segments (Supplementary Fig 6c-h)40. In any case, the rescue of all embryonic *Dact1* mutant phenotypes by concurrent mutation of *Vangl2* powerfully demonstrates that any E-cadherin or Wnt/β-catenin effects contributing to these phenotypes must occur downstream of Vangl2-dependent events.

We have discovered that a developmentally crucial function of Dact1 is regulation of Vangl2 at the PS. Morphogenetic abnormalities in the PS region of *Dact1* mutant embryos, while partly resembling those caused by PCP pathway reduction4, are unique in that they are associated with decreased phosphorylation of the myosin binding subunit of myosin phosphatase (Mypt1), but increased JNK activity. This agrees with evidence that modulations in Rho-and Jun-kinase activities reflect separate pathways downstream of PCP4, and that either abnormal gain or loss of upstream PCP components can cause similar disruptions in cell polarity, cytoskeletal dynamics, and CE movements41-44. Interestingly, other PCP phenotypes, such as inner ear and cardiac malformations18,45, are not evident in *Dact1* mutants (M. Montcouquiol, D.A.F., B.N.R.C., data not shown).

We propose that complex formation between the Dact1 and Vangl2 proteins is a crucial step in a novel Vangl2 regulatory pathway operating during EMT at the PS. Candidate cellular processes that might be involved include trafficking of Vangl2 to the membrane, endocytosis, subcellular sequestration, or degradation. This will be clarified by identifying additional components of this pathway through further biochemical, cellular, embryonic, and genetic experimentation.

METHODS

Targeting Construct

Approximately 7 kb of *Dact1* genomic DNA from the 129/Sv mouse strain was inserted into pGKneoF2L2DTA246 to create the *Dact1* targeting vector (Supplementary Fig 1). Correct targeting through homologous recombination in ES cells was confirmed by Southern blot and PCR. Mice carrying the targeted allele were created using standard embryo

manipulation and chimera breeding techniques. An allelic series at the *Dact1* locus was created by crossing to the *EIIa::Cre* (The Jackson Laboratory, Bar Harbor, ME) and FLPe transgenic mouse strains in order to excise loxP-flanked and FRT-flanked sequences respectively. Genotyping was performed by genomic PCR using allele-specific primers: The primers Dact1intron1 and Dact1intron2 (See Supplementary Table 4 for this and all other primer sequences) are separated by 689 bases of genomic sequence in wild type, but only 190 bases in the excised (mutant) allele; amplifying a mutant-specific PCR product of 243 bases. The primers Dact1exon2 (near start exon 2) and Dact1intron2 (near the start of intron 2) are both within the floxed region; amplifying a wild type-specific PCR product of 330 bases. Amplification parameters for wild type: 30 cycles X (95°C 30 seconds, 52°C 30 seconds, 72°C 30 seconds); for mutant: 38 cycles X (95°C 30 seconds, 57°C 30 seconds, 72°C 30 seconds).

Antibody generation

The Dact1 antibody was created by injecting rabbits with a peptide corresponding to aa 373-386 (coded within exon 4), followed by affinity purification. It is available from AbD Serotec.

General Microscopy and Imaging

As described14,40.

Skeleton Preparation

As described16.

Whole Mount mRNA in situ Hybridization

As described40 using LacZ probe to nucleotides 576-939 and previously established probes14,16,19,29.

LWR measurements

Whole Embryo Length to Width Ratio (LWR): Whole embryo length (L) was the average distance along a straight line to the posterior tip of the embryo from the anterior tips of the right and left head folds. Whole embryo width (W) was the distance between the lateral edges of the left and right somites positioned in the middle of the anterior-posterior axis (L/2). LWR was calculated as L/W.

Posterior Length to Width Ratio (LWR): Posterior length (L) was the average distance along a straight line to the posterior tip of the embryo from the posterior edges of the most posterior (last formed) left and right somites. Posterior embryo width (W) was the widest lateral distance across the embryo (perpendicular to L) in the region corresponding to L (posterior to the last formed somite). LWR was calculated as L/W.

Proliferation and Apoptosis measurements

To measure proliferation and apoptosis, embryos were sectioned and stained for phalloidin, Hoescht 33258, and phospho-histone-H3 (Millipore) or active caspase-3 (BD Biosciences),

respectively. Staining was visualized on a Nikon C1si Spectral Confocal microscope. A single confocal plane from each 20μm section was used to avoid double counting of cells. Graphs show the average percent proliferative or apoptotic cells across all sections (n = 2 embryos for each genotype, 5 sections per embryo) from the same genotype. There were no significant differences between mutants and controls for all these measures.

Quantitative RT-PCR

As described14 with the following modifications: Samples were embryonic tissues posterior to the last-formed somite. 0.5-1μg of total RNA was used for cDNA synthesis. Primers: QAxin2F, QAxin2R, QDll1F, QDll1R, QVangl2F, QVangl2R, QLacZF, QLacZR and for E-cadherin as described47.

JNK assay

Embryonic tissues posterior to the last-formed somite were homogenized in 100ul buffer and assayed as described26.

Western blots, CoIPs, GST pull-downs, expression and deletion constructs

Association assays were performed essentially as described48. GST pull downs were in PBS + 0.1% Triton-X-100 (Roche), 0.1% insulin. Binding was at 4°C for 30 minutes, followed by 3 X 5 minute washes in binding buffer at 4°C. ^{35}S-labelled in vitro translated proteins were synthesized in the TNT coupled wheat germ extract system (Promega). cDNAs were obtained commercially or by RT-PCR from wild type mouse total RNA. Expression and deletion plasmids were constructed using standard restriction digest and/or PCR techniques, and confirmed by sequencing. For Dvl2 the DS (pfam02377; aa 160-232), PDZ (cd00992; aa 265-352) and combined deletions are precise inverse PCR-mediated deletions of these domains as defined on the NCBI Uniprot website. The b (basic) domain is a conserved Arginine/Lysine-rich stretch located just upstream of the PDZ49, corresponds to aa 231-249 of mouse Dvl2, and is therefore distinct from the DS domain. Commercial antibodies (sources): Activated ß-Catenin “ABC” (Millipore)22, Vangl2, Dvl1, Dvl3, HA, FLAG (Santa Cruz Biotech), Dvl2 (Cell Signaling Technology), p120catenin (BD Biosciences), α-tubulin (Sigma-Aldrich), Phospho-Mypt (T696) (Millipore), Total Mypt1 (BD Biosciences).

Genotyping of Vangl2 and Wnt3a alleles

Vangl2^{Lp}—Genotyping for crosses was performed by *Crp* microsatellite PCR50. Genotypes of all combination mutant (experimental) and control littermates was verified by genomic PCR amplification and sequencing of alleles. Primers for PCR: Vangl2LpF and Vangl2LpR; for sequencing: Vangl2Lpseq.

Vangl2$^{Lp\text{-}m1Jus}$—Genotyping was performed by allele-specific PCR using primers homologous to the wild type versus the point mutant allele (Supplementary Fig 7). We used the primer pair Lp-m1JusWTF and Lp-m1JusWTR to amplify a 402 base pair wild type allele product using the following parameters: 30 cycles X (95°C 30 seconds, 68°C 30 seconds, 72°C 1 minute). We used the primer pair Lp-m1JusWT F and Lpm1JusMutR to

amplify a 402 base pair mutant allele product using the following parameters: 30 cycles X (95°C 30 seconds, 62°C 30seconds, 72°C 1 minute).

Wnt3a^{-} (Wnt3a^{neo})—Genotyping was performed by genomic PCR with allele-specific primers. Primers and parameters for the wild type allele were as recommended by the supplier (The Jackson Laboratory). We used primer pair Wnt3aneo and Wnt3aintron2 to amplify a *Wnt3a^{neo}*-specific 386 base pair product using parameters: 35 cycles X (95°C 30 seconds, 65°C 30 seconds, 72°C 1 minute).

IHC (Vangl2, E-cadherin)

Embryos were dissected in PBS, fixed in 4% paraformaldehyde for 1 hour at room temperature (RT), and washed in PBS. For embedding, embryos were incubated in 30% glucose in PBS at 4°C overnight, equilibrated with equal parts 30% glucose and O.C.T. compound (Tissue-Tek) for 2 hours on ice, then embedded in 30% glucose and O.C.T. compound. Embryos were cryosectioned (20μm) at -16°C. Sections were dried at RT, washed 2x in PBS for 5 minutes, blocked for 1.5 hour at RT using 10% heat inactivated goat serum, 1% BSA in PBS, then incubated in primary antibody overnight at 4°C. Rabbit Vangl2 antibody18 and Mouse E-cadherin antibody (BD Biosciences) were diluted 1:500 in 1% heat inactivated goat serum, 1% BSA in PBS. Sections were washed 5× 10 min in PBS, blocked, and incubated in anti-rabbit alexa fluor 488 and anti-mouse alexa fluor 568 (Molecular Probes) diluted 1:250 overnight at 4°C. Sections were washed 5×10 min in PBS, mounted in Mowiol and imaged via confocal microscopy under identical non-saturating illumination conditions.

IHC Quantitation

Signal intensity (grey scale) was measured using *ImageJ* software (NIH), across a straight line drawn parallel to the apical surface of the PS ectoderm and bisecting 5 adjacent cells. Pixel intensity was normalized to the lowest value along the entire line, which was set to 0 (background). For comparisons of cell surface intensity between cells, the 3 highest adjacent values corresponding to the two lateral cell surfaces (6 values total/cell) were averaged and plotted.

Statistical Analyses

All quantitative data were analyzed using Prism software (Graphpad). Significance was determined by parametric unpaired two-tailed t tests. In all cluster graphs, mean values are plotted as a horizontal line; numerical values for the mean, standard error, and p-value are reported in the corresponding **Results** text.

Supplementary Material

Refer to Web version on PubMed Central for supplementary material.

Acknowledgments

We thank all members of the Cheyette laboratory for thoughtful input and assistance with mouse husbandry and genetics. Eric P. Fox provided technical expertise for creation of the *Dact1* targeting construct, starting from the

pGKneoF2L2DTA2 vector donated by Philippe Soriano. ES cell manipulation and chimera production were accomplished at the University of Washington Transgenic Resources Program. Uta Grieshammer of the UCSF Department of Anatomy provided expert assistance with neonatal genitourinary phenotyping. Confocal microscopy was accomplished at the Nikon Imaging Center at UCSF/QB3, with advice from Kurt Thorn. Susan Dymecki provided the FLPe transgenic mouse line, Andrew McMahon the *Wnt3a* mutant mouse line, and Stefano Piccolo the BAT-gal line. Thomas Gridley provided probes for *Uncx4.1* and *Dll1*. Mireille Montcouquiol provided affinity-purified Vangl2 antibody. Anthony Wynshaw-Boris provided helpful comments on the final manuscript. BNRC gratefully acknowledges support from NIH R01HD055300, the Sandler Foundation, the UCSF Academic Senate Committee on Research, and the UCSF Center for Neurobiology and Psychiatry. R.S. is a recipient of a predoctoral fellowship from the California Institute of Regenerative Medicine. D.A.F. received support from the MSTP at Washington University St. Louis.

References

1. Yoshikawa Y, Fujimori T, McMahon AP, Takada S. Evidence that absence of Wnt-3a signaling promotes neuralization instead of paraxial mesoderm development in the mouse. Dev Biol. 1997; 183:234–42. [PubMed: 9126297]
2. Torban E, et al. Genetic interaction between members of the Vangl family causes neural tube defects in mice. Proc Natl Acad Sci U S A. 2008; 105:3449–54. [PubMed: 18296642]
3. Wang J, et al. Dishevelled genes mediate a conserved mammalian PCP pathway to regulate convergent extension during neurulation. Development. 2006; 133:1767–78. [PubMed: 16571627]
4. Ybot-Gonzalez P, et al. Convergent extension, planar-cell-polarity signalling and initiation of mouse neural tube closure. Development. 2007; 134:789–99. [PubMed: 17229766]
5. Veeman MT, Axelrod JD, Moon RT. A second canon: Functions and mechanisms of beta-catenin-independent wnt signaling. Developmental Cell. 2003; 5:367–377. [PubMed: 12967557]
6. Torban E, Wang HJ, Groulx N, Gros P. Independent mutations in mouse Vangl2 that cause neural tube defects in looptail mice impair interaction with members of the Dishevelled family. J Biol Chem. 2004; 279:52703–13. [PubMed: 15456783]
7. Huang H, He X. Wnt/beta-catenin signaling: new (and old) players and new insights. Curr Opin Cell Biol. 2008
8. Etheridge SL, et al. Murine dishevelled 3 functions in redundant pathways with dishevelled 1 and 2 in normal cardiac outflow tract, cochlea, and neural tube development. PLoS Genet. 2008; 4:e1000259. [PubMed: 19008950]
9. Zhang L, Gao X, Wen J, Ning Y, Chen YG. Dapper 1 antagonizes Wnt signaling by promoting dishevelled degradation. J Biol Chem. 2006; 281:8607–8612. [PubMed: 16446366]
10. Gloy J, Hikasa H, Sokol SY. Frodo interacts with Dishevelled to transduce Wnt signals. Nat Cell Biol. 2002; 4:351–7. [PubMed: 11941372]
11. Jiang X, et al. DACT3 is an epigenetic regulator of Wnt/beta-catenin signaling in colorectal cancer and is a therapeutic target of histone modifications. Cancer Cell. 2008; 13:529–41. [PubMed: 18538736]
12. Cheyette BNR, et al. Dapper, a Dishevelled-associated antagonist of beta-catenin and JNK signaling, is required for notochord formation. Dev Cell. 2002; 2:449–461. [PubMed: 11970895]
13. Lagathu C, et al. Dact1, a nutritionally regulated preadipocyte gene controls adipogenesis by co-ordinating the Wnt/{beta}-catenin signalling network. Diabetes. 2009; 58:609–619. [PubMed: 19073771]
14. Fisher DA, et al. Three Dact Gene Family Members are Expressed During Embryonic Development and in the Adult Brains of Mice. Dev Dyn. 2006; 235:2620–2630. [PubMed: 16881060]
15. Tam PP. A study of the pattern of prospective somites in the presomitic mesoderm of mouse embryos. J Embryol Exp Morphol. 1986; 92:269–85. [PubMed: 3723065]
16. Zhang N, Gridley T. Defects in somite formation in lunatic fringe-deficient mice. Nature. 1998; 394:374–7. [PubMed: 9690472]
17. Ikeya M, Takada S. Wnt-3a is required for somite specification along the anteroposterior axis of the mouse embryo and for regulation of cdx-1 expression. Mech Dev. 2001; 103:27–33. [PubMed: 11335109]

18. Montcouquiol M, et al. Asymmetric localization of Vangl2 and Fz3 indicate novel mechanisms for planar cell polarity in mammals. J Neurosci. 2006; 26:5265–75. [PubMed: 16687519]
19. Echelard Y, et al. Sonic hedgehog, a member of a family of putative signaling molecules, is implicated in the regulation of CNS polarity. Cell. 1993; 75:1417–1430. [PubMed: 7916661]
20. Aulehla A, et al. Wnt3a plays a major role in the segmentation clock controlling somitogenesis. Dev Cell. 2003; 4:395–406. [PubMed: 12636920]
21. Lickert H, et al. Dissecting Wnt/beta-catenin signaling during gastrulation using RNA interference in mouse embryos. Development. 2005; 132:2599–2609. [PubMed: 15857914]
22. Staal FJ, Noort Mv M, Strous GJ, Clevers HC. Wnt signals are transmitted through N-terminally dephosphorylated beta-catenin. EMBO Rep. 2002; 3:63–8. [PubMed: 11751573]
23. Park JI, et al. Frodo Links Dishevelled to the p120-Catenin/Kaiso Pathway: Distinct Catenin Subfamilies Promote Wnt Signals. Dev Cell. 2006; 11:683–695. [PubMed: 17084360]
24. Vandenberg AL, Sassoon DA. Non-canonical Wnt signaling regulates cell polarity in female reproductive tract development via van gogh-like 2. Development. 2009; 136:1559–70. [PubMed: 19363157]
25. Feng J, et al. Inhibitory phosphorylation site for Rho-associated kinase on smooth muscle myosin phosphatase. J Biol Chem. 1999; 274:37385–90. [PubMed: 10601309]
26. Hibi M, Lin A, Smeal T, Minden A, Karin M. Identification of an oncoprotein-and UV-responsive protein kinase that binds and potentiates the c-Jun activation domain. Genes Dev. 1993; 7:2135–48. [PubMed: 8224842]
27. Kibar Z, et al. Identification of a new chemically induced allele (Lp(m1Jus)) at the looptail locus: morphology, histology, and genetic mapping. Genomics. 2001; 72:331–7. [PubMed: 11401449]
28. Park M, Moon RT. The planar cell-polarity gene stbm regulates cell behaviour and cell fate in vertebrate embryos. Nat Cell Biol. 2002; 4:20–5. [PubMed: 11780127]
29. Kibar Z, et al. Ltap, a mammalian homolog of Drosophila Strabismus/Van Gogh, is altered in the mouse neural tube mutant Loop-tail. Nat Genet. 2001; 28:251–5. [PubMed: 11431695]
30. Le Douarin NM, Teillet MA, Catala M. Neurulation in amniote vertebrates: a novel view deduced from the use of quail-chick chimeras. Int J Dev Biol. 1998; 42:909–16. [PubMed: 9853821]
31. Hunter N, Hikasa H, Dymecki S, Sokol S. Vertebrate homologues of Frodo are dynamically expressed during embryonic development in tissues undergoing extensive morphogenetic movements. Dev Dyn. 2006; 235:279–84. [PubMed: 16278878]
32. Torban E, et al. Tissue, cellular and sub-cellular localization of the Vangl2 protein during embryonic development: effect of the Lp mutation. Gene Expr Patterns. 2007; 7:346–54. [PubMed: 16962386]
33. Devenport D, Fuchs E. Planar polarization in embryonic epidermis orchestrates global asymmetric morphogenesis of hair follicles. Nat Cell Biol. 2008; 10:1257–68. [PubMed: 18849982]
34. Pauli RM. Lower mesodermal defects: a common cause of fetal and early neonatal death. Am J Med Genet. 1994; 50:154–72. [PubMed: 8010347]
35. Stevenson RE, et al. Vascular steal: the pathogenetic mechanism producing sirenomelia and associated defects of the viscera and soft tissues. Pediatrics. 1986; 78:451–7. [PubMed: 3748679]
36. Manzoni GA, Ransley PG, Hurwitz RS. Cloacal exstrophy and cloacal exstrophy variants: a proposed system of classification. J Urol. 1987; 138:1065–8. [PubMed: 3656561]
37. Duesterhoeft SM, Ernst LM, Siebert JR, Kapur RP. Five cases of caudal regression with an aberrant abdominal umbilical artery: Further support for a caudal regression-sirenomelia spectrum. Am J Med Genet A. 2007; 143:3175–84. [PubMed: 17963219]
38. Ciruna B, Rossant J. FGF signaling regulates mesoderm cell fate specification and morphogenetic movement at the primitive streak. Dev Cell. 2001; 1:37–49. [PubMed: 11703922]
39. Nelson WJ, Nusse R. Convergence of Wnt, beta-catenin, and cadherin pathways. Science. 2004; 303:1483–7. [PubMed: 15001769]
40. Suriben R, Fisher DA, Cheyette BN. Dact1 presomitic mesoderm expression oscillates in phase with Axin2 in the somitogenesis clock of mice. Dev Dyn. 2006; 235:3177–83. [PubMed: 17013874]

41. Takeuchi M, et al. The prickle-related gene in vertebrates is essential for gastrulation cell movements. Curr Biol. 2003; 13:674–9. [PubMed: 12699625]
42. Park E, Kim GH, Choi SC, Han JK. Role of PKA as a negative regulator of PCP signaling pathway during Xenopus gastrulation movements. Dev Biol. 2006; 292:344–57. [PubMed: 16490187]
43. Veeman MT, Slusarski DC, Kaykas A, Louie SH, Moon RT. Zebrafish prickle, a modulator of noncanonical Wnt/Fz signaling, regulates gastrulation movements. Curr Biol. 2003; 13:680–5. [PubMed: 12699626]
44. Yan D, et al. Cell autonomous regulation of multiple Dishevelled-dependent pathways by mammalian Nkd. Proc Natl Acad Sci U S A. 2001; 98:3802–7. [PubMed: 11274398]
45. Phillips HM, et al. Disruption of planar cell polarity signaling results in congenital heart defects and cardiomyopathy attributable to early cardiomyocyte disorganization. Circ Res. 2007; 101:137–45. [PubMed: 17556662]
46. Hoch RV, Soriano P. Context-specific requirements for Fgfr1 signaling through Frs2 and Frs3 during mouse development. Development. 2006; 133:663–73. [PubMed: 16421190]
47. Hyenne V, et al. Vezatin, a protein associated to adherens junctions, is required for mouse blastocyst morphogenesis. Dev Biol. 2005; 287:180–91. [PubMed: 16199027]
48. Angers S, et al. The KLHL12-Cullin-3 ubiquitin ligase negatively regulates the Wnt-beta-catenin pathway by targeting Dishevelled for degradation. Nat Cell Biol. 2006; 8:348–57. [PubMed: 16547521]
49. Klingensmith J, et al. Conservation of dishevelled structure and function between flies and mice: isolation and characterization of Dvl2. Mechanisms of Development. 1996; 58:15–26. [PubMed: 8887313]
50. Copp AJ, Checiu I, Henson JN. Developmental basis of severe neural tube defects in the loop-tail (Lp) mutant mouse: use of microsatellite DNA markers to identify embryonic genotype. Dev Biol. 1994; 165:20–9. [PubMed: 8088438]

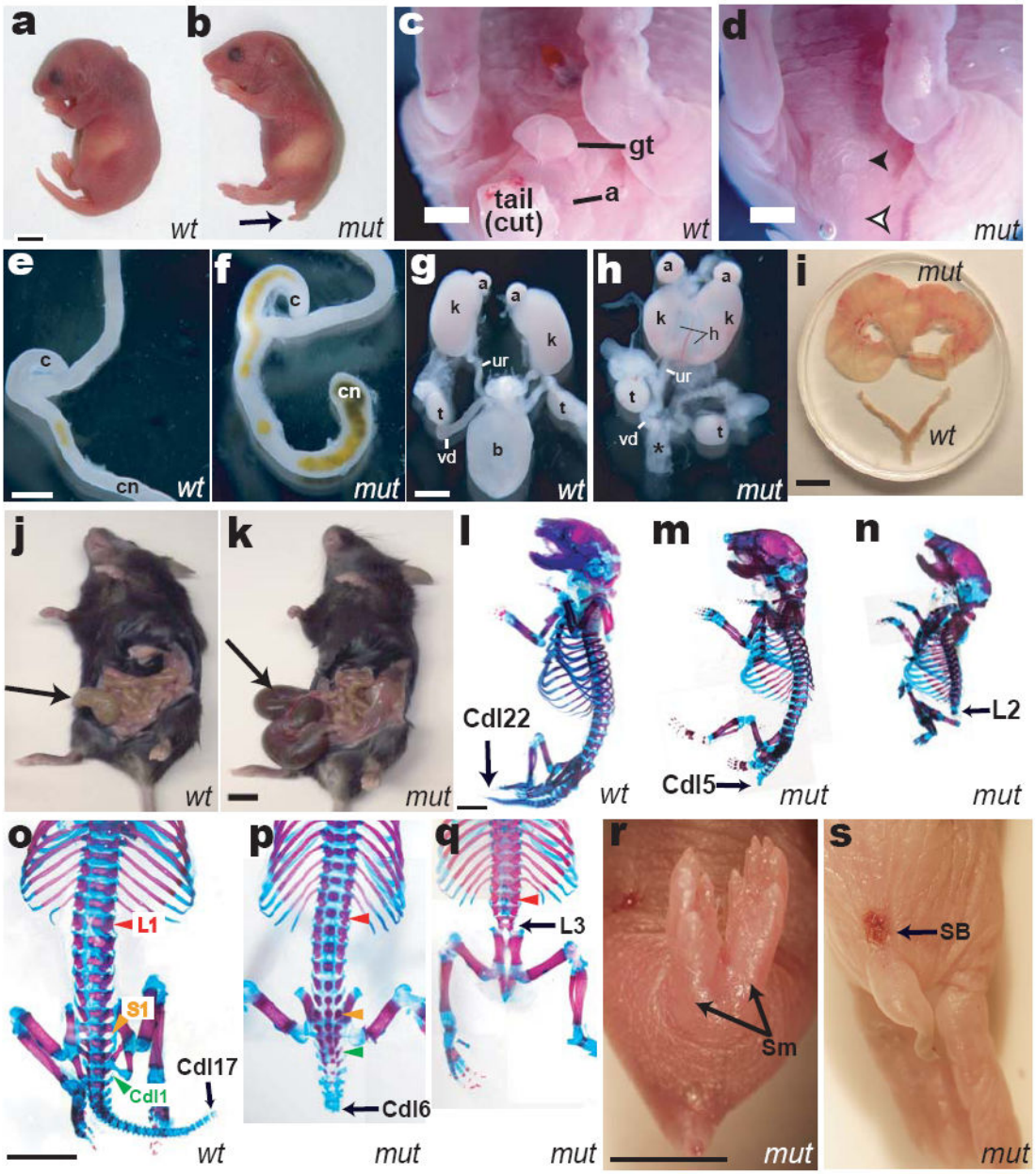

Figure 1.

Birth phenotypes in *Dact1* mutants (*mut*) compared to wild type (*wt*). **a, b** Outward appearance; arrow, short tail. **c, d** Genital tubercle (gt) and anus (a) are missing in mutants (filled arrowhead, empty arrowhead), along with the tail. **e, f** Mutants have a blind-ended colon (cn). **g, h** Mutants lack bladder (b *vs*. *), have malformed hydronephrotic (h) kidneys (k, fused in the mutant specimen), and misconnected ureters (ur, connected to the vas deferens (vd) in this mutant male). **i-k**, Phenotypes of rare surviving adult *Dact1* mutants consistent with impaired uterine outflow resulting in hydrometrocolpos (top *vs*. bottom in **i**), and impaired digestive tract evacuation resulting in megacolon (arrow in mutant **k** *vs*. wild type **j**). **l-q** Skeletons; black arrows indicate identity of the terminal ossified vertebra, colored arrowheads in **o-q** indicate segmental levels: red, lumbar-1 (L1); yellow, sacral-1

(S1); green, caudal-1 (Cdl1). **r** Sirenomelia (Sm). **s** Spina bifida (SB). Other abbreviations: (a) adrenal, (c) cecum, (t) testis. Scale bars: 0.5 mm, except i-k 5 mm.

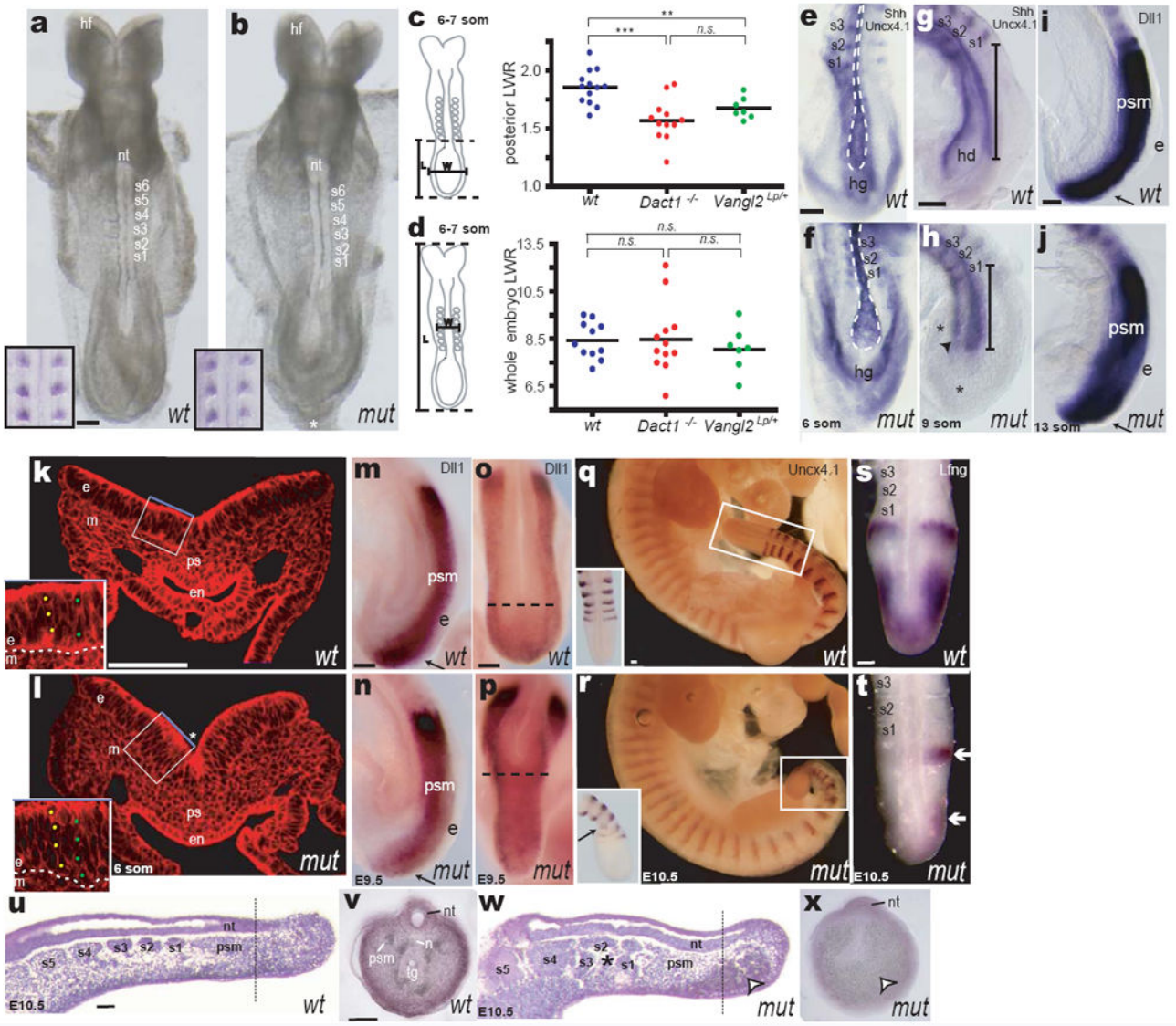

Figure 2.

Dact1 mutant embryonic phenotypes. **a, b** Early *Dact1* mutant (mut) embryos appear normal except for their posterior contour (*); insets: Uncx4.1 WISH (somites). **c, d** Length-Width-Ratio (LWR) measurements in wild type (blue), *Dact1* mutants (red) and *Vangl2*^{Lp} heterozygotes (green) posterior (**c**) or whole (**d**) embryo. **e-h** Shh/Uncx4.1 WISH. **e, f** ventral aspect; **g, h** lateral aspect. Notochord (outline in **e, f**; bracket in **g, h**) is shorter and broader in *Dact1* mutants compared to wild type. Hindgut diverticulum (hd in **g**) has not formed in mutant (arrowhead in **h**). Mesenchymal tissue (*) surrounds foreshortened axial structures. **i, j** Dll1 WISH: presomitic mesoderm (psm) and ectoderm (e, arrow) length are normal. **k, l** Phalloidin-stained transverse section at the primitive streak (ps). In mutant (**l**) endoderm (en) has not closed ventrally and is thinner, whereas ectoderm (e) is thicker (insets) and more sharply folded (*). **m-p** At later stages, Dll WISH (**m, n** lateral aspect; **o, p** dorsal aspect) reveals presomitic mesoderm and ectoderm of normal length (arrows), but less extended axial tissues (dotted lines). **q, r** Segmental abnormalities confined to the

newest somites in the tail bud (insets) can be detected by Uncx4.1 WISH at later stages (insets: close-up and dorsal view). **s, t** Somitogenic clock abnormalities in *Dact1* mutant tail buds revealed by abnormal asymmetric Lfng WISH (arrows). **u-x** Representative parasagittal (**u, w**); and transverse (**v, x**) sections through wild type (**u, v**) and *Dact1* mutant (**w, x**) tail buds at E10.5. *Dact1* mutants with abnormal somites (asterisk in **w**) also have severely disrupted posterior tissues and pooled blood at their ventral posterior tip (arrowhead in **w, x**); the neural tube (nt) nonetheless extends toward the tail bud tip. Dotted lines in **u, w** indicate approximate position of transverse sections from different embryos in **v, x**. Other abbreviations: (hf) head-folds, (s1-s8) somites, (hg) hindgut, (m) mesoderm, (n) notochord, (tg) tail gut. Scale bars = 0.1 mm. Statistical analysis (**c, d**): parametric unpaired two-tailed t test, horizontal line = mean; *n.s.* $p > 0.05$, $^{**}p < 0.01$, $^{***}p < 0.001$

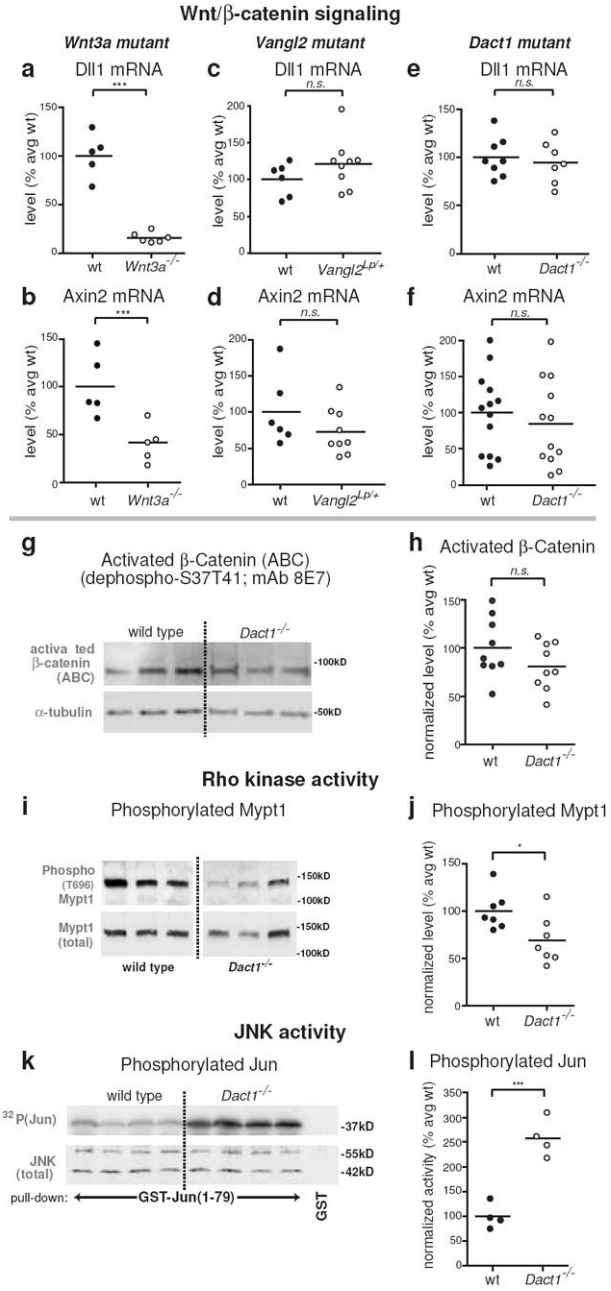

Figure 3.

Biochemical correlates of PCP signaling are specifically affected at early phenotypic stages. Insets: assays were conducted on posterior tissue lysates from E8 and E9 embryos as shown. All graphs: closed circles, wild type (+/+); open circles, mutant littermates. **a-h** Wnt/β-catenin assays. QPCR for endogenous targets of Wnt/β-catenin signaling at E8 reveals that Dll1 and Axin2 mRNA levels are significantly reduced in *Wnt3a null* embryos (**a, b**), but not in *Vangl2*^{Lp} heterozygotes (**c, d**), nor in *Dact1* mutants (**e, f**). Similarly, levels of unphosphorylated (activated) β-catenin protein are not significantly reduced in *Dact1* mutants at E9 (**g, h**). **i-l** PCP pathway biochemistry. Phosphorylation of Mypt1, a target of Rho kinase, is significantly reduced in *Dact1* mutants at E8 (**i, j**), whereas JNK activity is

robustly increased at E9 (**k, l**). Statistical analyses: parametric unpaired two-tailed t tests, horizontal line = mean; *n.s.* $p > 0.05$, *$p < 0.05$, ***$p < 0.001$

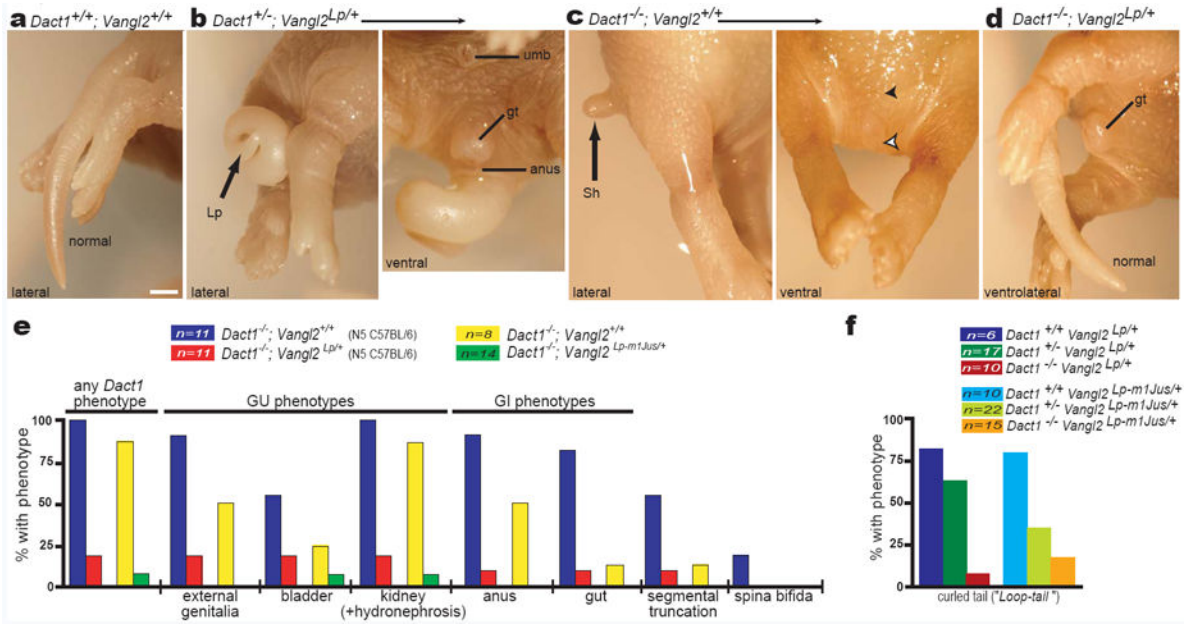

Figure 4.

Mutations in *Dact1* and *Vangl2* mutually rescue. **a-d** Posterior phenotypes of littermates from a *Dact1* × *Vangl2* mutant intercross. **a** $Dact1^{+/+};Vangl2^{+/+}$ neonate (wild type) has a normal tail. **b** $Dact1^{+/-};Vangl2^{Lp/+}$ neonate (trans-heterozygous) has a curly tail (Lp, left panel) typical of the semidominant *Loop-tail* phenotype, while the genital tubercle (gt) and anus (a) are normal (as expected for a *Dact1* heterozygote, right panel). **c** $Dact1^{-/-};Vangl2^{+/+}$ neonate has the shortened tail (Sh; left panel), absent genital tubercle and anus (filled and empty arrowheads, right panel) typical of *Dact1* mutants. **d** $Dact1^{-/-};Vangl2^{Lp/+}$ combination mutant neonate (genetically rescued mutant) has a normal genital tubercle (gt), anus (not shown), and tail. **e** Quantitation of phenotypes and affected organs in *Dact1* mutant littermates that either carry (red) or don't carry (blue) the $Vangl2^{Lp}$ allele, or that either carry (green) or don't carry (yellow) the $Vangl2^{Lp\text{-}m1Jus}$ allele (see also Supplementary Table 3a). **f** The *Dact1* mutant allele reciprocally rescues, in a dose-dependent manner, *Loop-tail* phenotypes produced by heterozygosity for either $Vangl2^{Lp}$ (left, darker bars) or $Vangl2^{Lp\text{-}m1Jus}$ (right, lighter bars) (see also Supplementary Table 3b). Other abbreviations: (umb) umbilicus. Scale bar: 1 mm.

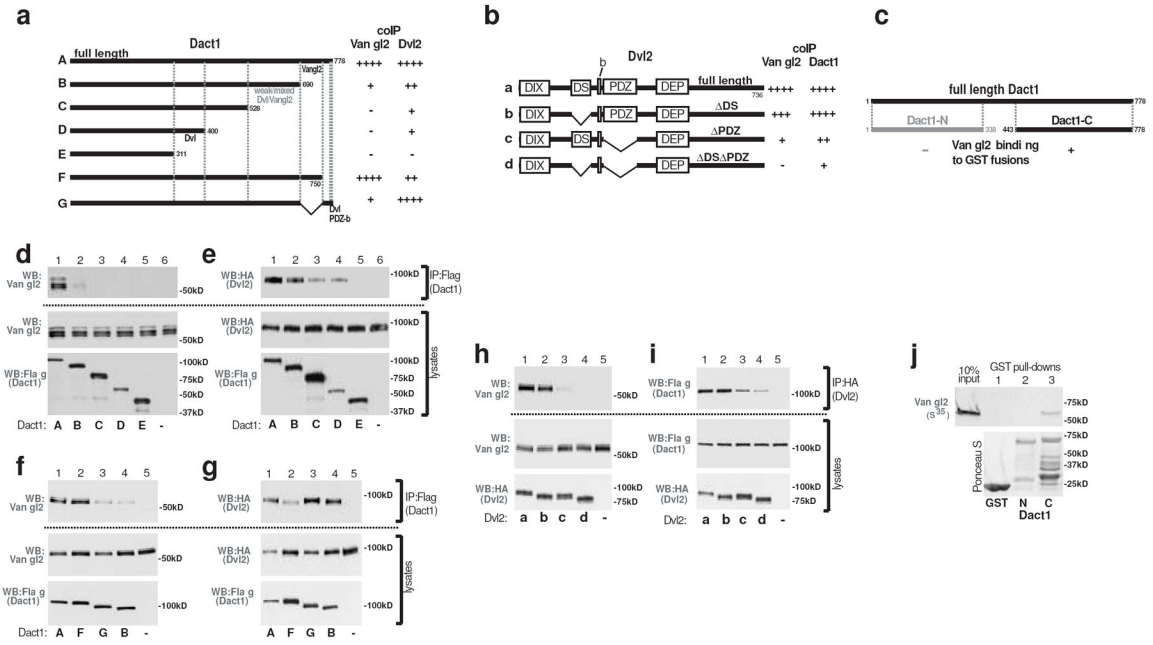

Figure 5.

The Dact1 and Vangl2 proteins associate independently of Dvl. **a-c** Schematic summaries of coIP and GST pull-down data. **d-i** coIPs of proteins recombinantly expressed in human embryonic kidney cells. **d** Vangl2 coIPs with full-length Dact1, but loses affinity as the Dact1 C-terminus is progressively deleted. **e** Dvl2 coIPs with Dact1 unless both the C-terminus and middle region are deleted. **f, g** Separate C-terminal subregions of Dact1 mediate coIP with Vangl2 (**f**) versus Dvl2 (**g**). **h** Vangl2 coIPs with full-length Dvl2 unless the Dvl2 PDZ domain is deleted; there is also a slight contribution from the Dvl2 DS domain. **i** Dact1 coIPs with Dvl2 even in the absence of both these domains. **j** A GST-fusion protein incorporating the Dact1 C-terminus binds to Vangl2 protein synthesized in a wheat germ extract with no Dvl proteins.

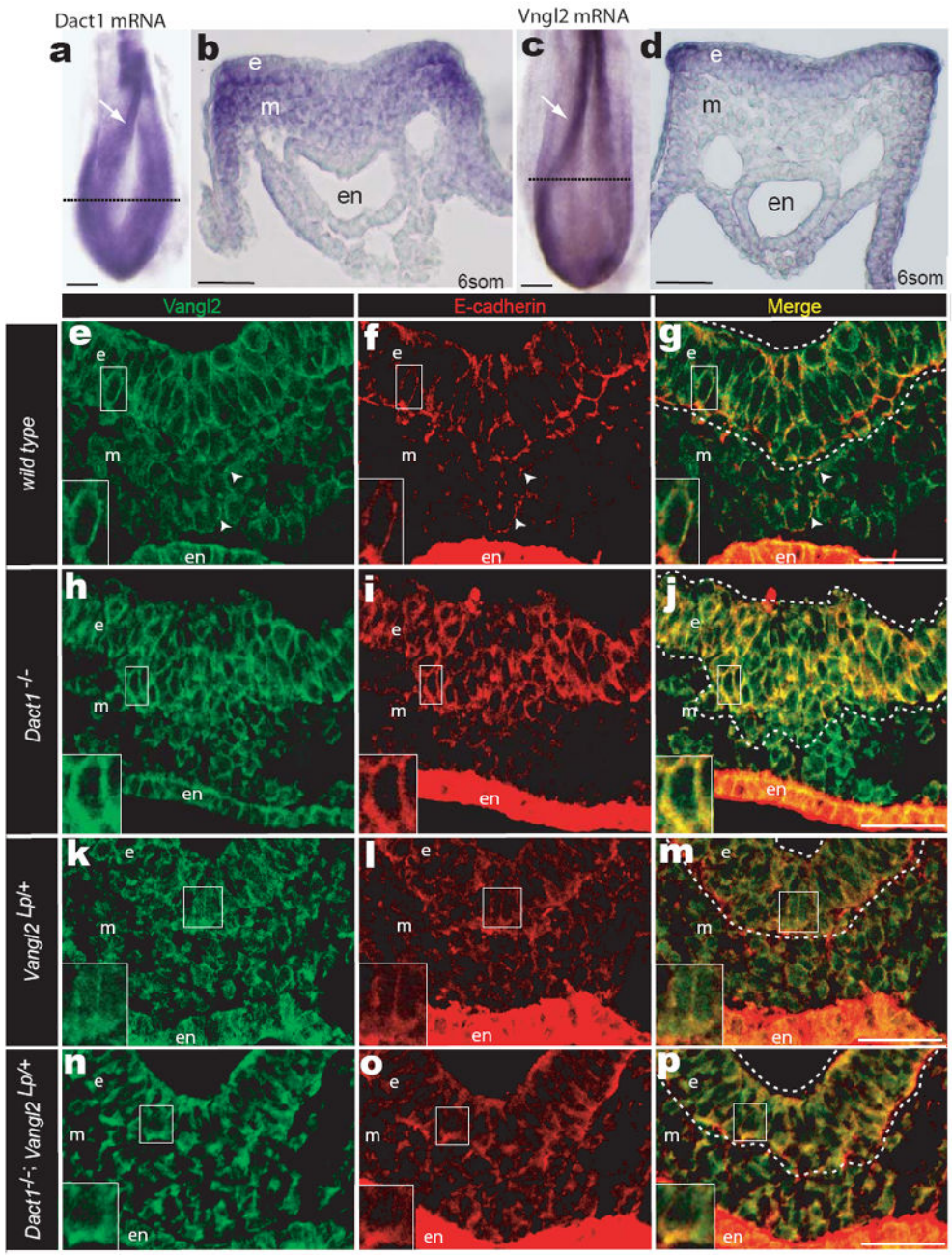

Figure 6.

Dact1 and Vangl2 functionally interact at the PS. **a, b** WISH Dact1 **c, d** WISH Vangl2 **a, c** Dorsal aspect showing neural fold (arrow) and approximate level of sections in **b** & **d** (dotted lines) **b, d** Transverse section at PS level. **e-p** Confocal fluorescent immunohistological localization of Vangl2 (green) and E-cadherin proteins (red) at the PS in *Dact1*$^{+/+}$;*Vangl2*$^{+/+}$ (wild type; **e-g**), *Dact1*$^{-/-}$;*Vangl2*$^{+/+}$ (*Dact1* mutant; **h-j**), *Dact1*$^{+/+}$;*Vangl2*$^{Lp/+}$ (*Loop-tail*; **k-m**), and *Dact1*$^{-/-}$;*Vangl2*$^{Lp/+}$ (genetically rescued mutant; **n-p**). Abbreviations as in Figure 2. Scale bars in **a-d** 0.1 mm, in **e-p** 0.05mm.